Microfluidic Control of Coexisting Chemical Microenvironments within Multiphase Water-in-Fluorocarbon Droplets

*Charles D. Crowe and Christine D. Keating**

Department of Chemistry, The Pennsylvania State University, University Park, Pennsylvania 16802, United States

Keywords: Microfluidics, Polymers, Phase Separation, Emulsions

Abstract

The use of aqueous polymer-based phase separation within water-in-oil emulsion droplets provides a powerful platform for exploring the impact of compartmentalization and preferential partitioning on biologically relevant solutes. By forming an emulsion, a bulk solution is converted into a large number of chemically isolated microscale droplets. Microfluidic techniques provide an additional level of control over the formation of such systems. This enables the selective production of multiphase droplets with desired solution compositions and specific characteristics, such as solute partitioning. Here, we demonstrate control over the chemical microenvironment by adjusting the composition to increase tie line length for poly(ethylene glycol) (PEG)-dextran aqueous two-phase systems (ATPS) encapsulated within multiphase water-in-fluorocarbon oil emulsion droplets. Through rational adjustment of microfluidic parameters alone, ATPS droplets

containing differing compositions could be produced during the course of a single experiment, with the produced droplets demonstrating a controllable range of tie line lengths. This provided control over partitioning behavior for biologically-relevant macromolecules such that the difference in local protein concentration between adjacent phases could be rationally tuned. This work illustrates a broadly applicable technique to rationally create emulsified multiphase aqueous systems of desired compositions through the adjustment of microfluidic parameters alone, allowing for easy and rapid screening of various chemical microenvironments.

Introduction

The field of aqueous phase separation has experienced a resurgence in recent years as it has been used to mimic crowded, compartmentalized cellular environments.[1–6] The ability to have simultaneously existing, yet chemically distinct, phases allows for a model of the multi-compartmental organization found *in vivo*.[7–11] To this end, several forms of phase separation, including the segregative phase separation of neutral polymers, have been incorporated into such systems.[6] Various reactions, including RNA catalysis,[12] bio-inspired mineralization,[13] and transcription/translation,[14,15] have been studied inside such environments, yielding both a better understanding of cellular mechanisms and additional experimental control over such reactions. As these experiments are performed within phase-separated aqueous solutions prepared as needed for each system, there is a great deal of control over the solution's chemical environment, such as polymer concentration and relative phase volume. Similarly, microfluidic methods have also been used to explore phase separation through the production of chemically isolated monodisperse emulsion droplets with controllable environments in the form of water-in-oil emulsions.[16–23] However, there has generally been little focus on controlling the specific composition of the

resulting aqueous phase-separated droplets, particularly with a goal of directing the resulting solution dynamics with regards to biomimetic applications. Since the polymer composition of the phase-separated system determines the partitioning of solutes within the solution, the ability to influence this aspect of the droplets is desirable. In this work, we have used microfluidics to produce multiphase aqueous water-in-fluorocarbon oil emulsion droplets, where the aqueous phase compositions, resulting tie line lengths, and solute partitioning behavior may be rationally controlled through variations of microfluidic parameters alone (Figure 1A).

The physical chemistry governing bulk aqueous phase separation has been explored for decades, particularly as a means of using neutral polymer or polymer/salt aqueous two phase systems (ATPS) in biological separations, as included solutes typically demonstrate preferential partitioning among the phases present.[24–28] Given an arbitrary two phase system, a phase diagram maps the total polymer compositions that result in either single phase or phase-separated solutions. For any composition within the phase-separated region, there exists a tie line connecting it to two points on the binodal line, which give the polymer composition of the individual phases (Figure 1B).[24,25,29,30] The tie line length (TLL) reflects the disparity in composition between the two phases; longer tie lines indicate more distinct phases, and lead to stronger solute partitioning.[3,26,31–35] Solute localization within distinct coexisting aqueous phases, both as a bulk system and as droplets, has been extensively studied for use in applications such as biomolecular purification and extraction,[24,36–40] bioengineering,[28,41–43] modeling of membraneless organelles,[11,44–48] and reactant localization.[12–14,49] Such phase-separated systems have also been studied in the form of emulsions, recently in conjunction with microfluidic technologies, resulting in the production of both all-aqueous[18,19,21,50–53] and water-in-oil[54–57] emulsions with controllable morphologies, surface

chemistry, and encapsulated components. However, while TLL has long been used as a means of controlling local solute concentration within bulk ATPS,[24,27,32,34,38,39] such efforts have generally not been undertaken for droplet-based systems, due to the difficulty in selecting specific phase compositions on an individual droplet level.

Here, we have used microfluidics to selectively produce ATPS-containing water-in-fluorocarbon oil emulsions with specific TLL, giving us influence over the partitioning of biological solutes within the coexisting aqueous phases. We chose poly(ethylene glycol) (PEG) and dextran (Figure S1) as the phase-separation driving polymers, due to their well-understood segregative phase-separation behavior. The oil and surfactants used in this work were adapted from previously published work and utilize the fluorinated oil HFE-7500 with a water-soluble, positively-charged polyetherdiamine (Jeffamine ED-900) and a fluorocarbon-soluble, negatively-charged carboxylated perfluoropolyether (Krytox 157 FSH) (Figure S2).[58] We selected an emulsion system containing a fluorocarbon oil-based continuous phase due to its potential in future work to encapsulate biological reactions, as water-in fluorocarbon oil emulsions have been used extensively in such applications due to their minimal molecular transport between droplets.[58–61] The methods and techniques discussed here are not limited to this specific system and could be adopted for other water-in-oil emulsion systems, such as those containing a hydrocarbon oil-based continuous phase. We have demonstrated that biomolecular solute partitioning behavior can be tuned through control over microfluidic variables alone. This additional level of control will advance the design of cellular mimics, as well as the ability to screen multiple ATPS compositions for desired characteristics with a single experimental setup.

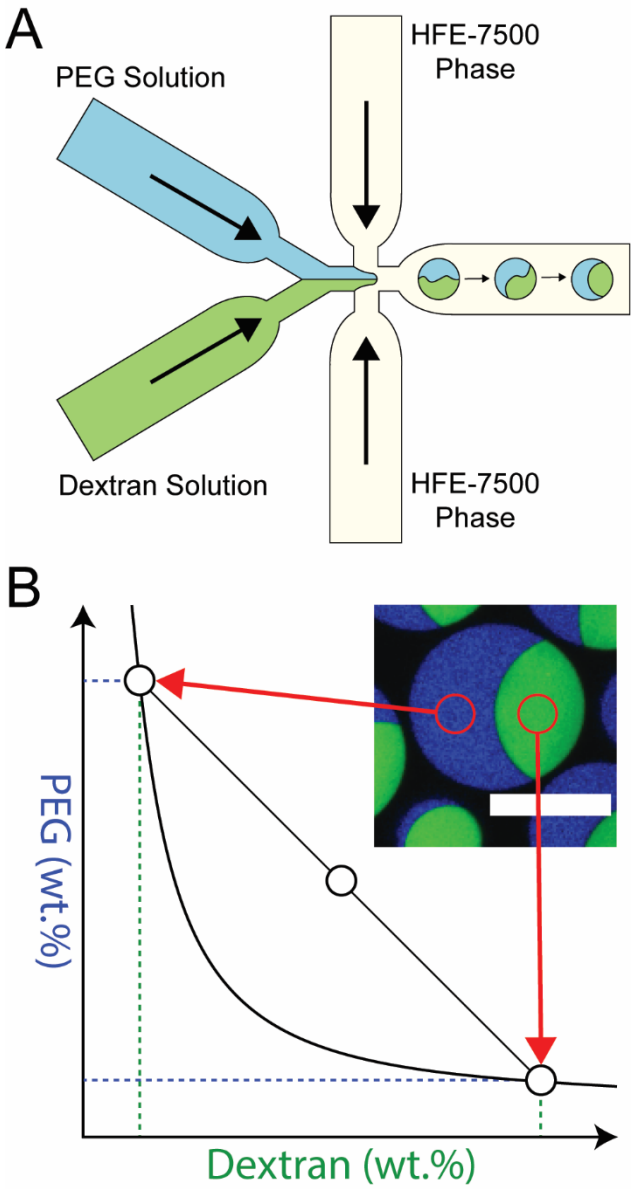

Figure 1: Overview of droplet production and measurement methodology. (a) Schematic of microfluidic setup showing the production of multiphase water-in-fluorocarbon oil emulsion droplets. (b) Fluorescence intensity measurements of each phase are used to quantify polymer concentration, leading to the mapping of a phase diagram. Inset: overlaid fluorescence image shown. Dextran Alexa Fluor 488 (false colored green) and PEG Alexa Fluor 647 (false colored blue). Scale bar 100 μm.

Materials and Methods:

Materials

Poly(ethylene glycol) (MW 8 kDa), Dextran from *Leuconostoc mesenteroides* (average MW 9 kDa to 11 kDa), Jeffamine ED-900 (O,O′-Bis(2-aminopropyl) polypropylene glycol-*block*-polyethylene glycol-*block*-polypropylene glycol), HEPES (N-(2-Hydroxyethyl)piperazine-N′-(2-ethanesulfonic acid)), methanol, Ficoll PM 70 (MW 70 kDa) (Figure S1), 40 kDa Ficoll-TRITC (polysucrose 40-tetramethylrhodamine isothiocyanate, average MW 30 kDa to 50 kDa), 400 kDa Ficoll-TRITC (polysucrose 400-tetramethylrhodamine isothiocyanate, average MW 350 kDa to 450 kDa), catalase from bovine liver (lyophilized powder, 2,000-5,000 units/mg protein), 3-(1,1-dimethyl-2-hydroxyethyl)-3-amino-2-hydroxypropanesulfonic acid (AMPSO), sodium chloride (NaCl, anhydrous), and Tris buffered saline were purchased from Sigma-Aldrich, Co. (St. Louis, MO). Magnesium chloride hexahydrate and ammonium hydroxide were purchased from EMD Millipore (Burlington, MA). HFE 7500 was acquired from 3M (Maplewood, MN) and TMC Industries (Waconia, MN). Krytox 157 FSH was purchased from Miller-Stephenson (Danbury, CT). Dextran Alexa Fluor 488 (MW 10 kDa) and Fluorescein-5-Isothiocyanate (FITC) were purchased from ThermoFisher Scientific (Waltham, MA). BSA-TRITC (albumin from bovine serum (BSA), tetramethylrhodamine conjugate) and ConA-TRITC (concanavalin A, tetramethylrhodamine conjugate) were purchased from Invitrogen (Eugene, Oregon). m-PEG37-NHS ester was purchased from BroadPharm (San Diego, CA). Details regarding the preparation of PEG Alexa Fluor 647 and PEG-catalase-FITC, which were produced in-house, are found in Text S1.

Fluorocarbon Oil Phase Preparation

The water-in-fluorocarbon oil emulsion system used was adapted from previously published literature and was selected for its high stability and biocompatibility, as well as ease of production.[58,62] The oil phase consisted of the fluorocarbon oil HFE 7500 with 1.8 wt.% Krytox 157 FSH ammonium salt. The Krytox 157 FSH was converted to its ammonium salt to ensure a negative charge on its carboxylate headgroup. A mixture of 10 wt.% Krytox in methanol was prepared, resulting in a cloudy solution with pH ~5. Ammonium hydroxide was added drop-wise until the pH was above 7, at which point the Krytox partially precipitated from solution. The methanol was decanted and was completely removed by blowing nitrogen gas over it and leaving it under vacuum. The resulting Krytox was an extremely viscous liquid, which was dissolved in HFE 7500 to 1.8 wt.%.

Forming Emulsions via Vortex Mixing

To prepare multiphase aqueous emulsions from bulk ATPS, first individual solutions of PEG and dextran were prepared. The following method was used for both polymer solutions. The polymer was dissolved into solution (5 mM HEPES, 1 mM $MgCl_2$) at 40 wt.%, before being mixed using both a vortex mixer and a rotisserie until fully dissolved (typically overnight). Then, 1 mL of the solution was transferred to a separate container. The Jeffamine was slightly warmed to ensure it was completely liquid, before it was added to the polymer solution to a final concentration of 0.71 vol.%. Additionally, the appropriate labeled polymer (either PEG Alexa Fluor 647 or dextran Alexa Fluor 488) was added to a final concentration of 0.25 vol.%. This solution was then mixed completely via vortex mixing. A separate solution of only 5mM HEPES, 1 mM $MgCl_2$, and 0.71 vol.% Jeffamine was also prepared.

The bulk ATPS were prepared by mixing appropriate masses of the 40 wt.% PEG, 40 wt.% dextran, and non-polymer containing solutions to achieve the desired final compositions. These were then mixed completely using a vortex mixer. The final emulsions were prepared by mixing 200 μL of the previously prepared fluorocarbon oil phase (HFE 7500 with 1.8 wt.% Krytox) with 100 μL of the ATPS, which was pipette mixed before addition to ensure homogeneity during emulsion formation. The emulsion was formed by vortex mixing for 15 seconds.

Forming Emulsions via Microfluidics

When performing a microfluidic experiment, the stock 40 wt.% polymer and non-polymer containing solutions were prepared as described above. These were then used to prepare 20 wt.% solutions of each polymer by mixing equal masses of the 40 wt.% polymer solution with the non-polymer containing solution. These were mixed completely and used as the starting aqueous solutions for the microfluidic trials.

Full details regarding the microfluidic system are found in Text S2. Two separate reservoirs containing fluorocarbon oil phase were attached to the top and bottom inlets of the 2-reagent droplet chip (100 μm etch depth, hydrophobic coating) (Dolomite Microfluidics, Royston, UK), while the PEG and dextran solutions were connected to the middle two inlets (Figure 1A). The pressure of all reservoirs was slowly increased until flow was observed in all channels. The pressure of each channel was set to 500 mbar and the droplet production was allowed to stabilize for 5 minutes (Figure S3B). Following this, the pressures could be adjusted, always keeping the both fluorocarbon oil-containing channels at 500 mbar, and the total aqueous pressure at 1000 mbar. Samples were collected within Eppendorf tubes only after at least 1 minute had passed

following the change in pressure settings, to ensure all droplets produced under the previous setting were clear of the device and outflow tubing. Droplets were collected for at least 1 minute to ensure a large enough population to image. When complete, the microfluidic chip was cleaned by flowing water, ethanol, and air through it respectively.

Quantifying Phase Composition Using Confocal Microscopy

All fluorescence and transmitted light images were acquired using a Leica (Wetzlar, Germany) TCS SP5 PL confocal microscope using a HC PL APO 20x/0.75 CS2 objective, using Leica LAS-X software. Images were analyzed using ImageJ (National Institutes of Health).

The concentration of PEG and dextran in solution was determined by relating each polymer's relative dilution compared to its starting stock solution (40 wt.%), which contained a known amount of fluorescently labeled polymer. First, calibration curves of both PEG and dextran were obtained. Each polymer solution was prepared as described above, at 40 wt.% polymer and 0.25 vol.% labeled polymer solution. Using this starting stock and a non-polymer solution prepared as described above, solutions of 35 wt.%, 30 wt.%, 25 wt.%, 20 wt.%, 15 wt.%, 10 wt.%, 5 wt.%, and 0 wt.% were also prepared. These were emulsified in the fluorocarbon oil phase and observed using confocal microscopy. Sequential scanning was used to ensure that each labeled polymer's emission did not interfere with the collection of the other dyes. Scanning settings were optimized to ensure maximum intensity at 40 wt.%. At least three images of droplets were acquired for each concentration. Then, using ImageJ, the average fluorescence intensity of 30 droplets (10 from each image) was recorded, as well as the intensity of the background (also 30 measurements), which was subtracted from the fluorescence intensity. This was repeated for each solution, resulting in a

range of fluorescence intensity. This was related to the relative dilution of the starting solution (e.g. the 20 wt.% sample had a relative dilution of 0.5 from the starting 40 wt.% stock) in order to account for slight variations in the starting concentration of the stock solution in future trails. Calibration curves were obtained using this method for both the PEG and dextran solutions (Figure S4).

When phase-separated droplets were observed, three images were acquired sequentially using both the PEG and dextran scan settings. Then four measurements were obtained from each set of droplets: PEG intensity in the PEG-rich phase, PEG intensity in the dextran-rich phase, dextran intensity in the PEG-rich phase, and dextran intensity in the dextran-rich phase. The background intensity for both images was also measured. Each measurement consisted of 30 individual droplets (10 from each image). After background subtraction, the calibration curves for each polymer were used to determine the dilution of each phase relative to the starting PEG and dextran solutions, and subsequentially the concentration of PEG and dextran in each phase. Additionally, the tie line length (TLL) of each phase composition was calculated using:

$$TLL = \sqrt{(C_{dex,dex-rich} - C_{dex,PEG-rich})^2 + (C_{PEG,dex-rich} - C_{PEG,PEG-rich})^2} \quad (1)$$

where $C_{dex,dex\text{-}rich}$ and $C_{dex,PEG\text{-}rich}$ are the concentrations of dextran in the dextran-rich phase and PEG-rich phase, respectively, and $C_{PEG,dex\text{-}rich}$ and $C_{PEG,PEG\text{-}rich}$ are the concentrations of PEG in the dextran-rich phase and PEG-rich phase, respectively

Determining Partitioning of Solutes within Emulsion Droplets

The partitioning of solutes was explored using 40 kDa Ficoll TRITC, 400 kDa Ficoll TRITC, BSA-TRITC, ConA-TRITC, and PEG-catalase-FITC. As the TRITC and FITC fluorescence

emission overlapped with the previously collected dextran Alexa 488 scan when the 488 nm laser line was used, it was necessary to obtain a separate dextran calibration curve with a reduced emission collection window. The calibration curve was otherwise obtained as described above, ensuring that minimal TRITC fluorescence was visible.

Stock solutions of each solute were prepared at the highest reasonable concentration viable given their respective solubilities. This was done to ensure the brightest possible signal when the final ATPS droplets were viewed using microscopy. Each stock solution was prepared in a solution with 5 mM HEPES and 1 mM $MgCl_2$. Ficoll 40 kDa TRTIC was prepared at 3 mM, Ficoll 400 kDa TRITC at 0.6 mM, BSA-TRITC at 0.6 mM, and ConA-TRITC at 10 mg/mL. Despite repeated mixing, some solid remained present in the ConA-TRITC stock solution, as expected.[63] Additionally, as Ficoll can also phase-separate in the presence of PEG, dextran, or both,[14,25,64,65] sufficiently low concentration was selected to avoid this, with each solution visually checked for turbidity to ensure no phase separation had occurred. The PEG-catalase-FITC solution was prepared in-house, and the exact concentration was not determined. Instead, the solution was repeatedly concentrated using a 10 kDa molecular weight cut-off centrifugal filter until sufficiently concentrated to achieve a strong fluorescence microscopy image.

To explore partitioning, the solutes of interest were added to the 40 wt.% polymer solutions and non-polymer containing solution (which were prepared as described above) at a concentration of 0.5 vol.% (from the stock solutions described above). This was done to ensure that the concentration of solute was equal between both solutions in the microfluidic reservoirs, and so would remain constant despite changing PEG:dextran solution mixing ratios.

After droplet production, the droplets were imaged as described above, with an addition scan for the labeled solute fluorescence. Then, the fluorescence intensity was measured for each phase (with background subtraction) as described above (with 30 measurements total). For 40 kDa Ficoll TRITC, 400 kDa Ficoll TRITC, and BSA-TRITC, where the solute fluorescence was similar within all droplets, the effective partitioning coefficient (K) was calculated by dividing the average intensity of the fluorescent solute in the PEG-rich phase (I_{PEG}) by the average intensity in the dextran-rich phase ($I_{dextran}$):

$$K = \frac{I_{PEG}}{I_{dextran}} \tag{2}$$

ConA-TRITC and PEG-catalase-FITC resulted in droplets with a distribution of intensity, likely due to aggregation leading to uneven inclusion of solute between individual droplets. For these, the effective partitioning coefficient was calculated for individual droplets first, before being averaged for each sample, as the partitioning coefficient is not concentration-dependent and is the same for each droplet with identical phase compositions.

To calculate the change in concentration of each solute within the individual droplet phases with varying PEG:dextran pressure ratio, first the droplet morphology was measured, resulting in the calculated volume ratio of the PEG-rich and dextran-rich phases, as detailed in Text S3. Then, the concentration of solute in each phase was calculated by first determining the concentration in the dextran-rich phase using the starting bulk concentration (C_{bulk}) of each solute, the calculated PEG-rich:dextran-rich volume ratio (R_V), and the measured effective partitioning ratio (K):

$$C_{dextran} = \frac{C_{bulk}(1+R_v)}{1+K*R_v} \tag{3}$$

Then, the concentration in the PEG-rich phase was calculated using

$$C_{PEG} = K * C_{dextran} \quad (4)$$

Results and Discussion

To explore the microfluidic production of multiphase water-in-oil emulsion droplets with controllable solution microenvironments, we selected the well-understood ATPS of PEG (MW 8 kDa) and dextran (MW 10 kDa)[3,24,25] and produced an emulsion using a fluorocarbon oil-based continuous phase.[58] As our microfluidic platform, we chose to use a pre-manufactured glass chip designed to mix two solutions to form the interior of the droplets, allowing us to change the pressure of each polymer solution, and thus their mixing (Figure 1A).

We first show a means to quantify the resulting aqueous phase compositions of the droplets through fluorescence microscopy alone by measuring the intensity of fluorescently-labeled moieties of the polymers participating in phase separation. We then apply this technique onto droplets created through microfluidics, exploring the degree of control we have over phase composition through the manipulation of microfluidic parameters alone. Finally, we examine how this influence manifests in the partitioning of various biologically-relevant macromolecular solutes.

Measuring Bulk-Prepared ATPS Phase Composition

In order to validate the measurement of phase composition via fluorescence microscopy (as described in Text S4), the method was first explored using bulk PEG-dextran ATPS of known concentration in the form of multiphase water-in-fluorocarbon oil emulsion droplets. By preparing

the ATPS before emulsification, the total concentration of PEG and dextran could be specified. Then, after measuring the concentration of the phases using the calibration curves obtained above, the resulting tie line length could be calculated and subsequently plotted as a phase diagram, where the tie lines could be compared to the known bulk compositions. Additionally, non-phase-separated samples were explored, to verify the method regardless of phase separation behavior. Eighteen bulk concentrations were chosen, spanning across both the single-phase and phase-separated regions of the phase diagram, ranging from 6 wt.% PEG/3 wt.% dextran to 20 wt.% PEG/20 wt.% dextran.

Of the chosen concentrations, four samples did not phase separate and an additional sample (8 wt.% PEG/8 wt.% dextran) exhibited a mix of phase separated and non-phase separated droplets. This final sample likely contained a bulk composition of polymers extremely close to the binodal, resulting in slight variations in polymer composition shifting phase behavior drastically. As such, it was excluded from measurements. For the remaining non-phase-separated samples, the concentration of PEG and dextran calculated from the fluorescence intensity agreed well with the known bulk concentration (Figure S6A).

The samples with polymer concentrations high enough to cause phase separation were imaged and the concentration of PEG and dextran was measured in both phases. Two samples (15 wt.% PEG/15 wt.% dextran and 20 wt.% PEG/20 wt.% dextran) demonstrated at least one phase with a fluorescence higher than that accounted for in the calibration range, indicating that the polymers were concentrated above 40 wt.%. As these were outside of calibration, they were not included in further analyses. When the remaining phase compositions were calculated, the resulting tie lines

could be measured and plotted, where they formed a distinct phase diagram with a clear binodal line (Figure S6C). Additionally, when the known bulk concentrations of the ATPS were plotted, they fell close to the tie lines drawn between the phase compositions measured with microscopy, indicating a good agreement between the two methods (Figure S6A).

To demonstrate the range of the phase diagram that could be explored with this technique, we prepared samples containing equal bulk concentrations of PEG and dextran ranging from 9 wt.% PEG/9 wt.% dextran to 14 wt.% PEG/14 wt.% dextran. As the bulk concentration increased, the resulting phase compositions become more distinct, visualized on a phase diagram as extending further out into the phase-separated region (Figure 2A), and within microscopy images as an increasing contrast in fluorescence between the two phases. The resulting length of the tie lines were quantified as a means of determining the degree of chemical dissimilarity between the two phases. As the composition of the bulk ATPS changed, so did the TLL, increasing as the bulk concentrations increased (Figure 2B).

In order to determine whether this technique could be used to select the desired phase composition of a given droplet system, we prepared a series of compositions expected to have the same tie line length, using the phase diagram generated by the bulk ATPS to select potential bulk concentrations of PEG and dextran (Figure 2C). Although these bulk ATPS contained widely varying total concentrations of each polymer, they demonstrated similar TLL, indicating that the final compositions of each phase after phase separation were very similar (Figure 2D).

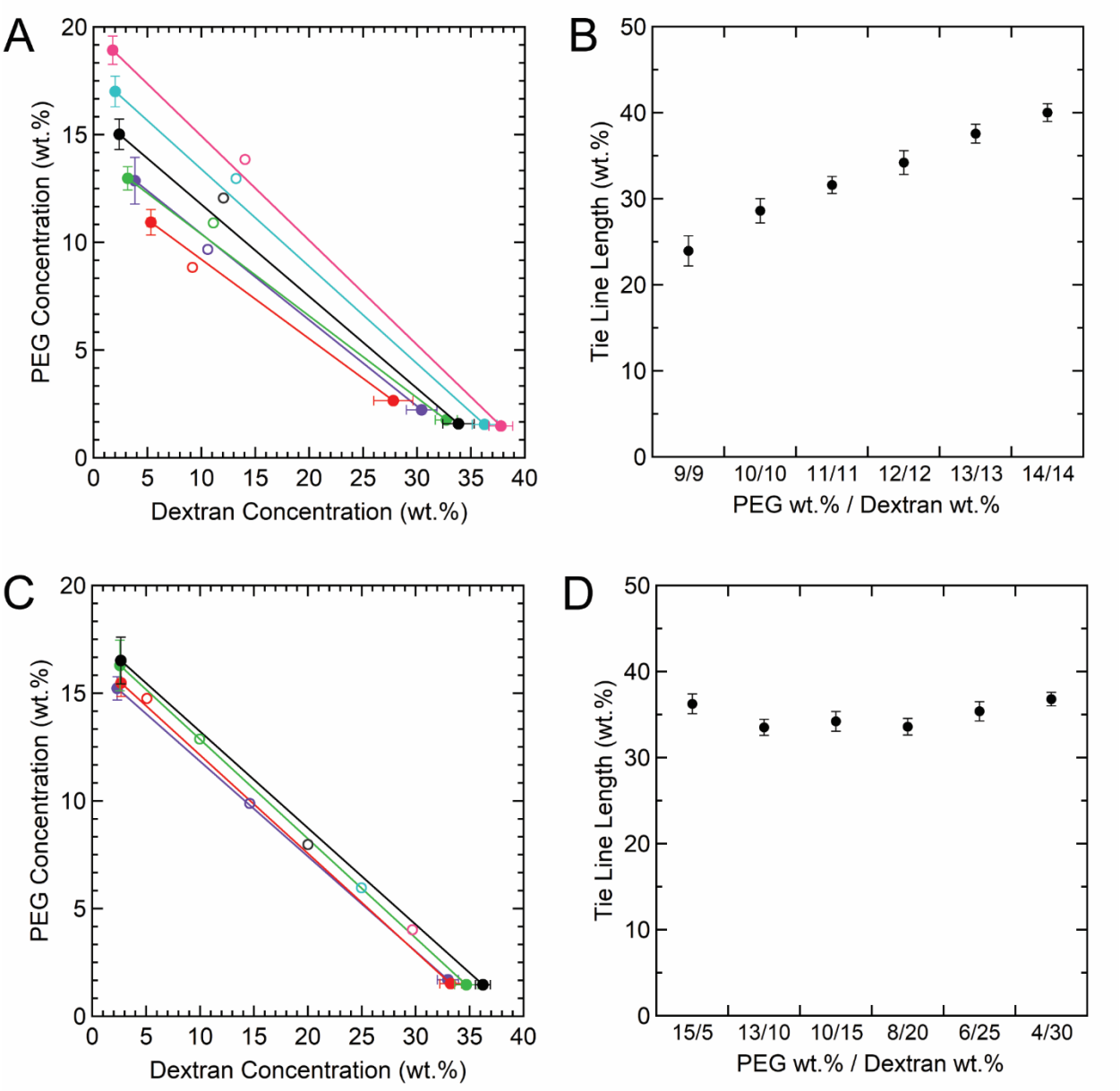

Figure 2: Measuring TLL of varying phase compositions. (a) Prepared ATPS bulk compositions (open circles) and associated experimentally-measured phase compositions (closed circles) from samples with equal bulk concentrations of PEG and dextran. (b) Calculated tie line length of phase-separated compositions in (a). (c) Known ATPS bulk compositions (open circles) and associated experimentally-measured phase compositions (closed circles) from samples along a single tie line. (d) Calculated tie line length of phase-separated compositions in (c).

Microfluidic Production of ATPS Droplets

When producing an ATPS via the mixing of two solutions, the amount of each solution incorporated into the resulting system determines the final bulk phase composition of the ATPS, as each solution dilutes the other. To control this with microfluidics, we separated the PEG and dextran solutions and specified the pressure applied to each, thus governing the degree of mixing. Although the concentration of PEG and dextran in the microfluidic reservoirs remained constant, this variation in mixing allowed us to scan through compositions with varying TLL by changing the amount of each solution incorporated into the final droplets. Practically, this was determined by the ratio of pressures applied to each fluid, which we express as $R_{PEG:dextran}$ (defined as the pressure of the PEG solution divided by the pressure of the dextran solution). In order to simplify the influencing factors between different pressure configurations, the total aqueous pressure was set constant at 1000 mbar (i.e., $P_{PEG} + P_{dextran} = 1000$ mbar). The pressure of the fluorocarbon oil phase was also kept constant, with both reservoirs maintained at 500 mbar.

Droplets were produced over a range of $R_{PEG:dextran}$ from 0.5 to 5, with sixteen total pressure ratios explored. After collection, confocal microscopy confirmed that each produced a monodisperse population of droplets. Droplets produced with a $R_{PEG:dextran}$ at or below 0.8 were not phase separated, indicating that the resulting concentrations of PEG and dextran was located in the single-phase region of the phase diagram (Figure 3, left). However, for $R_{PEG:dextran}$ at or above 0.9, phase separation was observed, with clearly complete phase separation occurring at $R_{PEG:dextra}$ of 1.25 (Figure 3, middle). As the pressure of the PEG solution increased, more PEG was incorporated into the droplets, lengthening the resulting TLL as the resulting droplet composition shifted further into the two-phase region on the phase diagram. Additionally, the relative phase

volumes of the droplets changed, with the PEG-rich phase contributing more to the droplets' volume as $R_{PEG:dextran}$ increased (Figure 3, right).

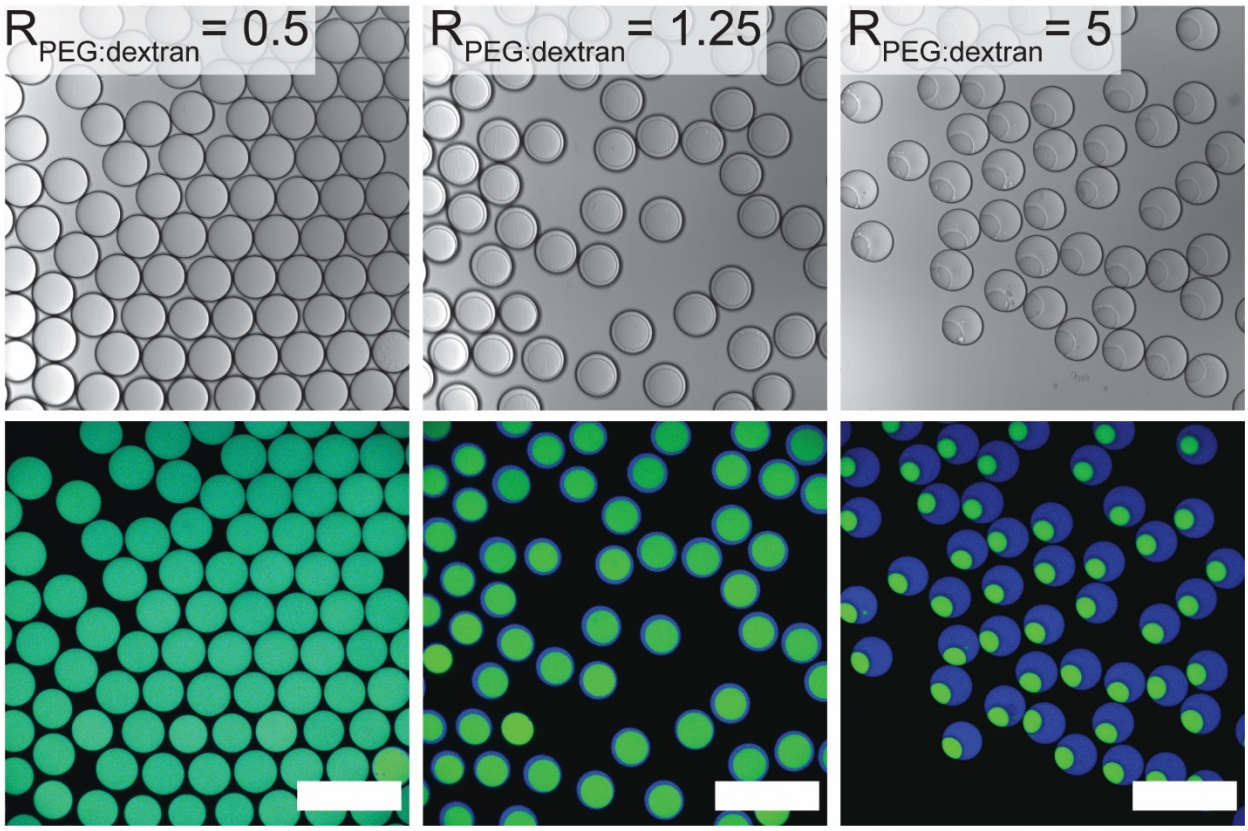

Figure 3: Laser scanning confocal microscopy images of water-in-fluorocarbon oil emulsion droplets produced via microfluidics at varying PEG:dextran pressure ratios. Fluorescence channels have been false colored and overlaid, with the brightness adjusted for viewing: PEG Alexa Fluor 647 (blue) and dextran Alexa Fluor 488 (green). Scale bar 200 μm.

When the compositions of the phases were measured, they were again found to form the binodal line of a phase diagram (Figure 4A). As $R_{PEG:dextran}$ increased, the phase compositions shifted further into the phase-separated region of the phase diagram, confirming that the variation in pressure ratio resulted in a variation of solution incorporation into the droplets, changing the final composition and the resulting TLL. Accordingly, the PEG:dextran effective partitioning ratio was calculated for the included fluorescently labeled PEG and dextran, showing that each partitioned

more strongly into their respective polymer-rich phase as the PEG:dextran pressure ratio was increased (Figure 4B) This was further quantified by calculating the length of the tie lines for each set of droplets produced, which was compared to the set PEG-dextran pressure ratio (Figure 4C). As $R_{PEG:dextran}$ increased, the length of the tie lines also increased.

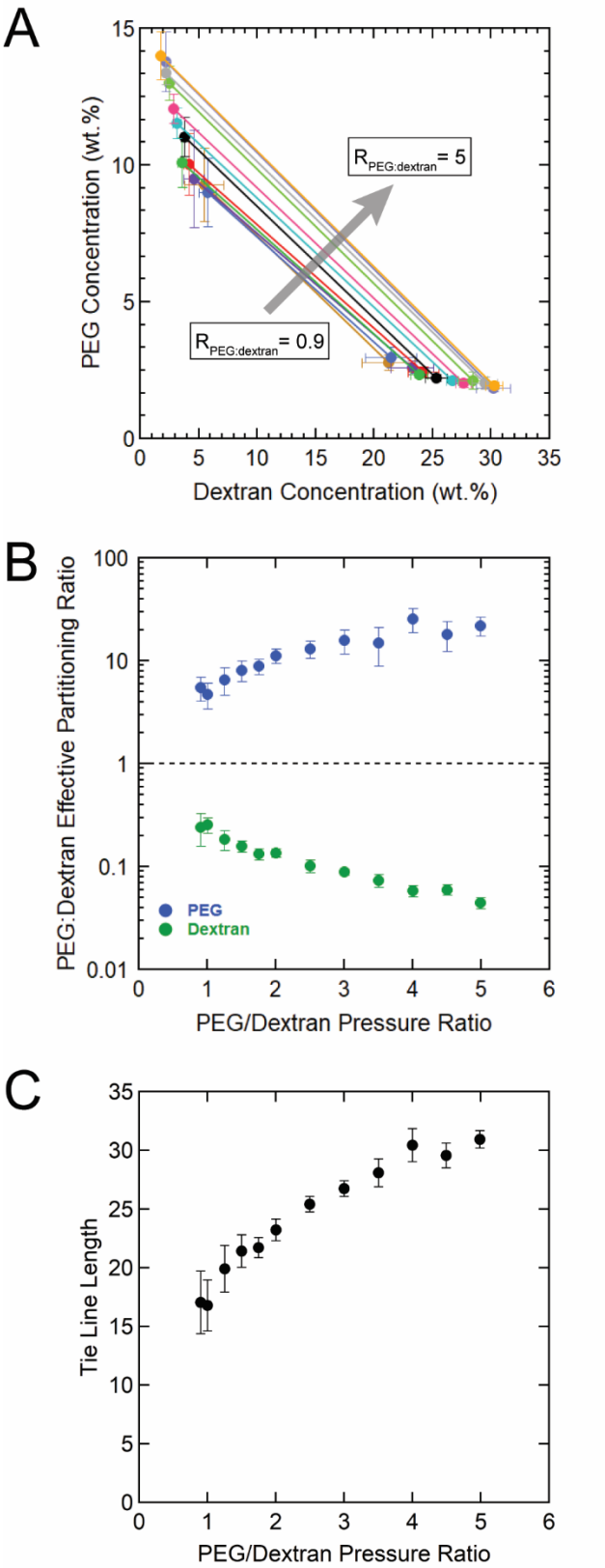

Figure 4: Polymer composition and phase behavior of phase-separated PEG:dextran ATPS water-

in-fluorocarbon oil emulsion droplets produced via microfluidics. (a) Measured phase composition of produced ATPS emulsion droplets ranging from $R_{PEG:dextran}$ of 0.9 to 5. (b) Partitioning of PEG Alexa Fluor 647 (blue) and dextran Alexa Fluor 488 (green) within phase-separated droplets vs. the PEG:dextran pressure ratio used to produce the droplets. (c) Graph of calculated tie line length vs. the PEG:dextran pressure ratio used to produce the droplets.

Controlling Partitioning Behavior with Microfluidic Parameters

In order to examine how our control over the TLL of the polymer phase composition within the multiphase droplets translated into control of solute partitioning and concentration, we selected solutes which are known to have preferential partitioning within PEG-dextran ATPS. This partitioning was quantified as an effective partitioning coefficient, which was calculated by taking the ratio between the fluorescently labeled solutes' intensity in the PEG-rich phase and the intensity in the dextran-rich phase. First, we examined solutes expected to partition into the more hydrophilic dextran-rich phase. Ficoll, a highly branched polysucrose, was an ideal candidate, as it is chemically similar to dextran, a glucan (Figure S1). Additionally, we selected both 40 kDa and 400 kDa Ficoll, as partitioning is also dependent on solute size, with larger solutes generally exhibiting stronger partitioning.[24,37,66,67] Previous observations without our lab have demonstrated its preference for the dextran-rich phase of a PEG/dextran ATPS, making it an ideal starting point for examining our control over partitioning strength.

The experimental trails with Ficoll TRITC (40 kDa and 400 kDa) were prepared such that the concentration of the solute was equal in both the PEG and dextran starting solutions, to ensure equal incorporation across all $R_{PEG:dextran}$. While emulsions were produced with $R_{PEG:dextran}$ ranging from 0.5 to 5, only those droplets produced with $R_{PEG:dextran}$ greater than or equal to 1.25

demonstrated phase separation. This was the case for all emulsions prepared with additional solutes. This differed from the emulsions prepared without additional solutes, where a $R_{PEG:dextran}$ of 0.9 was required for phase separation. Likely, the inclusion of the solutes shifted the location of the binodal line such that a different polymer composition was required for phase separation to occur.

Ficoll partitions to the dextran-rich phase, resulting in $K < 1$. Here, Ficoll 40 kDa TRITC demonstrated an effective partitioning coefficient of 0.78 ± 0.6 at the lowest $R_{PEG:dextran}$ (1.25), which decreased to 0.61 ± 0.4 as $R_{PEG:dextran}$ was increased to 5 (Figure 5C). This relatively modest ~1.3-fold increase in partitioning strength was within the error of our measurements. In contrast, Ficoll 400 kDa TRITC exhibited not only a stronger partitioning overall, but a larger change, as its partitioning began at 0.40 ± 0.05 before reducing to 0.16 ± 0.02, resulting in a 2.5-fold increase in partitioning strength. This difference between the 40 kDa and 400 kDa MW Ficoll reflected the expected trend of larger molecular weight solutes generally showing stronger partitioning.[37,66,67]

Additionally, we selected several well-explored proteins (BSA and ConA) to serve as representative biomacromolecules and demonstrate the ability to partition and concentrate biologically relevant solutes. These fluorescently labeled solutes, BSA-TRITC and ConA-TRITC, were included similarly to the Ficoll 40 kDa TRITC and Ficoll 400 kDa TRITC described above, starting at an equal concentration in the PEG and dextran solutions. After droplet production, the BSA-TRITC showed a 2.9-fold increase in partitioning strength, decreasing from 0.55 ± 0.08 to 0.19 ± 0.03. The ConA-TRITC yielded the largest change, starting at a partitioning coefficient of 0.33 ± 0.09 before reducing to 0.05 ± 0.02, a 6.6-fold increase in partitioning strength (Figure 5B).

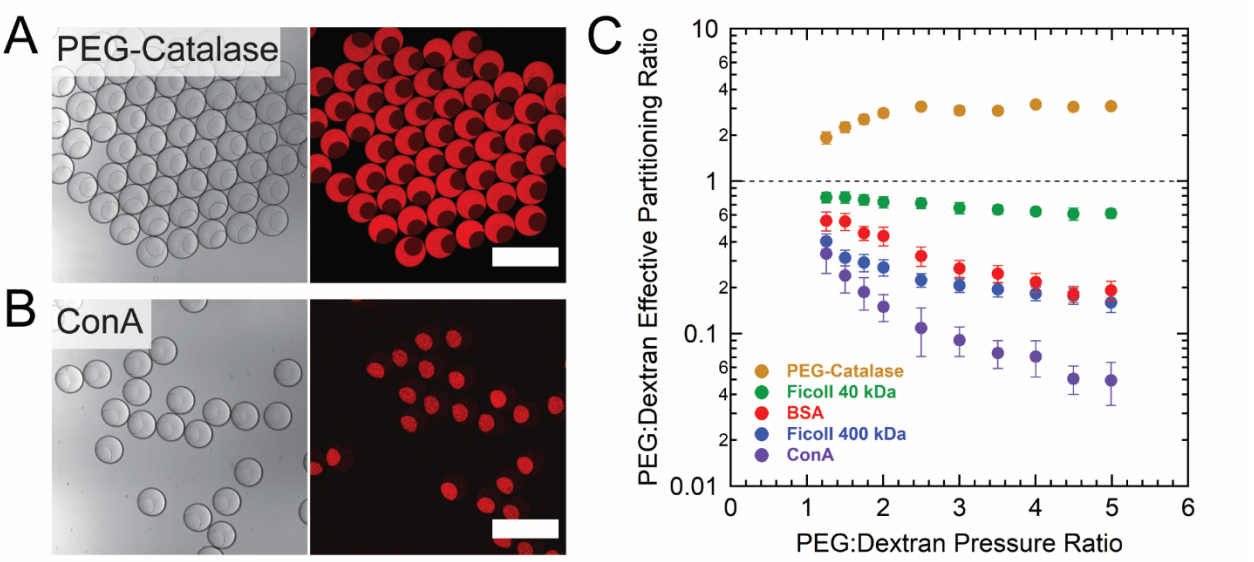

Figure 5: Partitioning of fluorescently labeled solutes within ATPS emulsion droplets. (a) Example microscopy image of PEG-catalase-FITC partitioning within PEG:dextran ATPS emulsion droplets ($R_{PEG:dextran}$ = 2.5). The fluorescence channel has been false colored red. Scale bar 200 μm. (b) Example microscopy image of Concanavalin A-TRITC partitioning within PEG:dextran ATPS emulsion droplets ($R_{PEG:dextran}$ = 3). The fluorescence channel has been false colored red. Scale bar 200 μm. (c) Graph showing effective partitioning of fluorescently labeled solutes within PEG:dextran ATPS multiphase droplets vs. the PEG:dextran pressure ratio used to produce the emulsions.

As all of these solutes exhibited preferential partitioning into the dextran-rich phase of the produced PEG/dextran ATPS emulsion droplets, we selected a final solute to demonstrate the ability to control the partitioning of solutes within the PEG-rich phase. Because all of the solutes tested above partitioned into the dextran-rich, we selected a PEGylated protein as the final solute of interest: PEG-catalase-FITC. After incorporation into the droplets, we observed partitioning into the PEG-rich phase, as expected, and measured the partitioning coefficient at 1.9 ± 0.2 when

$R_{PEG:dextran}$ was 1.25. At $R_{PEG:dextran}$ of 5, the partitioning coefficient had increased to 3.1 ± 0.2, showing a 1.6-fold increase in partitioning strength (Figure 5A).

In addition to experimentally determining the effective partitioning ratio of each solute using fluorescence intensity, the concentrations of the solutes within the individual phases were also estimated at both the lowest $R_{PEG:dextran}$ of 1.25, and the highest of 5. As $R_{PEG:dextran}$ was changed, not only did the phase compositions and resulting solute partitioning behavior change, but also the relative volumes of the PEG-rich and dextran-rich phases. These individual volumes were estimated using microscopy images and used to calculate the volume ratio between the two phases (Figure S5). Using these values, as well as the known starting concentration of each solute in the bulk samples and the effective partitioning ratios, the estimated local solute concentration in both phases was calculated (Tables S1 and S2). All solutes for which the starting bulk concentration was known (excluding PEG-catalase) showed an increase in local concentration within their preferential phase when $R_{PEG:dextran}$ was increased, reflecting the increase in partitioning strength also observed above (Figure S7, Tables S1 and S2). The largest increase in local concentration was demonstrated by ConA, which had begun at a starting bulk concentration of 0.05 mg/mL. This was increased to 0.088 ± 0.015 mg/mL in the dextran-rich phase with a PEG:dextran pressure ratio of 1.25, and further concentrated to 0.31 ± 0.04 mg/mL at the highest PEG:dextran pressure ratio of 5.

Conclusions

We have demonstrated how tie-line length can be used to rationally control the distribution of biomolecular solutes within phase-separated aqueous droplets produced via microfluidics. Multiphase aqueous water-in-fluorocarbon oil emulsion droplets were created with control over

their final phase composition and resulting partitioning behavior via rational adjustments to the microfluidic parameters used to create them. This was accomplished through the microfluidic selection of specific ATPS compositions with varying tie line lengths, measured using fluorescence confocal microscopy to quantify the concentration of PEG and dextran in both aqueous phases. After determining the relation between microfluidic parameters (i.e. PEG:dextran pressure ratio) and the resulting ATPS tie line length, the chemical microenvironments of the final multiphase emulsion droplets could be chosen, allowing the adjustment of solute partitioning behavior within them via microfluidic changes alone.

The control afforded by the ability to design ATPS w/o emulsion droplets with a desired composition has obvious implications in the incorporation of reactions. Tuning the partitioning coefficient of reagents between phases allows for influence over local concentration, reaction initiation, and reaction rate.[4] While this facilitates the modeling of the cellular environment's compartmentalization, it also could have importance in the fine-tuning of systems without direct mimicry in mind as well, such as the reaction of biomineralization, where partitioning and droplet morphology are critically important to the final mineral formed.[13] We intend for these results to provide a tool that enables directed design of multiphase systems for potential applications within the broad fields that utilize aqueous phase separation.

ASSOCIATED CONTENT

The following files are available free of charge.

Chemical structures of polymers used for phase separation and partitioning; chemical structures of the components of the fluorocarbon oil-based phase; overview of microfluidic setup;

calibration curve information for PEG and dextran solutions; calculated PEG:dextran volume ratio of selected droplets; measurement of polymer composition of bulk single-phase and phase-separated droplets; calculated concentration of solutes within selected droplets; tables of droplet characteristics for solute-containing systems; method of preparing fluorescently labeled compounds; description of microfluidic system; method of determination of multiphase droplet morphology; description of polymer composition quantification through fluorescence microscopy (PDF)

AUTHOR INFORMATION

Corresponding Author

*E-mail: keating@chem.psu.edu

ORCID

Charles D. Crowe: 0000-0002-9353-5340

Christine D. Keating: 0000-0001-6039-1961

Author Contributions

CDC performed the experiments. CDC and CDK designed the experiments and interpreted the data. The manuscript was written through contributions of all authors. All authors have given approval to the final version of the manuscript.

Funding Sources

This work was supported by the National Science Foundation, grant MCB-1715984.

Notes

The authors declare no competing financial interest.

ACKNOWLEDGMENT

We would like to thank Dr. Richard Booth for his preparation of the PEG-Catalase-FITC used within the partitioning studies within this work. This work was supported by the National Science Foundation, grant MCB- 1715984.

ABBREVIATIONS

AMPSO, 3-(1,1-dimethyl-2-hydroxyethyl)-3-amino-2-hydroxypropanesulfonic acid; ATPS, aqueous two-phase system; BSA, bovine serum albumin; ConA, concanavalin A; FITC, Fluorescein isothiocyanate; HEPES, (N-(2-Hydroxyethyl)piperazine-N′-(2-ethanesulfonic acid)); kDa, kilodalton; mPEG-amino, poly(ethylene glycol) methyl ether amine; MW, molecular weight; PEEK, polyether ether ketone; PEG, poly(ethylene glycol); RNA, ribonucleic acid; TLL, tie line length; TRITC, tetramethylrhodamine isothiocyanate; OD, outer diameter.

REFERENCES

(1) Alberti, S. Phase Separation in Biology. *Curr. Biol.* **2017**, *27* (20), R1097–R1102. https://doi.org/10.1016/j.cub.2017.08.069.

(2) Zhu, Y.; Guo, X.; Liu, J.; Li, F.; Yang, D. Emerging Advances of Cell-Free Systems toward Artificial Cells. *Small Methods*. John Wiley and Sons Inc October 20, 2020, p 2000406. https://doi.org/10.1002/smtd.202000406.

(3) Keating, C. D. Aqueous Phase Separation as a Possible Route to Compartmentalization of Biological Molecules. *Acc. Chem. Res.* **2012**, *45* (12), 2114–2124. https://doi.org/10.1021/ar200294y.

(4) Nakashima, K. K.; Vibhute, M. A.; Spruijt, E. Biomolecular Chemistry in Liquid Phase Separated Compartments. *Front. Mol. Biosci.* **2019**, *6*, 21. https://doi.org/10.3389/fmolb.2019.00021.

(5) Yeh Martín, N.; Valer, L.; Mansy, S. S. Toward Long-Lasting Artificial Cells That Better Mimic Natural Living Cells. *Emerg. Top. Life Sci.* **2019**, ETLS20190026. https://doi.org/10.1042/ETLS20190026.

(6) Crowe, C. D.; Keating, C. D. Liquid–Liquid Phase Separation in Artificial Cells. *Interface Focus* **2018**, *8* (5), 20180032. https://doi.org/10.1098/rsfs.2018.0032.

(7) Strom, A. R.; Brangwynne, C. P. The Liquid Nucleome - Phase Transitions in the Nucleus at a Glance. *J. Cell Sci.* **2019**, *132* (22), jcs.235093. https://doi.org/10.1242/jcs.235093.

(8) Shorter, J. Phasing in and Out. *Nat. Chem.* **2016**, *8* (6), 528–530. https://doi.org/10.1038/nchem.2534.

(9) Hondele, M.; Heinrich, S.; De Los Rios, P.; Weis, K. Membraneless Organelles: Phasing out of Equilibrium. *Emerg. Top. Life Sci.* **2020**, *4* (3), 343–354. https://doi.org/10.1042/ETLS20190190.

(10) Takinoue, M.; Takeuchi, S. Droplet Microfluidics for the Study of Artificial Cells. *Analytical and Bioanalytical Chemistry*. 2011, pp 1705–1716. https://doi.org/10.1007/s00216-011-4984-5.

(11) Martin, N. Dynamic Synthetic Cells Based on Liquid–Liquid Phase Separation. *ChemBioChem* **2019**, *20* (20), 2553–2568. https://doi.org/10.1002/cbic.201900183.

(12) Strulson, C. A.; Molden, R. C.; Keating, C. D.; Bevilacqua, P. C. RNA Catalysis through Compartmentalization. *Nat. Chem.* **2012**, *4* (11), 941–946. https://doi.org/10.1038/nchem.1466.

(13) Rowland, A. T.; Cacace, D. N.; Pulati, N.; Gulley, M. L.; Keating, C. D. Bioinspired Mineralizing Microenvironments Generated by Liquid-Liquid Phase Coexistence. *Chem. Mater.* **2019**, *31* (24), 10243–10255. https://doi.org/10.1021/acs.chemmater.9b04275.

(14) Torre, P.; Keating, C. D.; Mansy, S. S. Multiphase Water-in-Oil Emulsion Droplets for Cell-Free Transcription–Translation. *Langmuir* **2014**, *30* (20), 5695–5699. https://doi.org/10.1021/la404146g.

(15) Sokolova, E.; Spruijt, E.; Hansen, M. M. K.; Dubuc, E.; Groen, J.; Chokkalingam, V.; Piruska, A.; Heus, H. A.; Huck, W. T. S. Enhanced Transcription Rates in Membrane-Free Protocells Formed by Coacervation of Cell Lysate. *Proc. Natl. Acad. Sci.* **2013**, *110* (29), 11692–11697. https://doi.org/10.1073/pnas.1222321110.

(16) Keller, S.; Teora, S. P.; Boujemaa, M.; Wilson, D. A. Exploring New Horizons in Liquid Compartmentalization via Microfluidics. *Biomacromolecules*. American Chemical Society May 10, 2021, pp 1759–1769. https://doi.org/10.1021/acs.biomac.0c01796.

(17) Hardt, S.; Hahn, T. Microfluidics with Aqueous Two-Phase Systems. *Lab Chip* **2012**, *12* (3), 434–442. https://doi.org/10.1039/C1LC20569B.

(18) Choi, D.; Lee, E.; Kim, S.-J.; Han, M. Passive Droplet Generation in Aqueous Two-Phase Systems with a Variable-Width Microchannel. *Soft Matter* **2019**, *15* (23), 4647–4655. https://doi.org/10.1039/C9SM00469F.

(19) Moon, B.-U.; Abbasi, N.; Jones, S. G.; Hwang, D. K.; Tsai, S. S. H. Water-in-Water Droplets by Passive Microfluidic Flow Focusing. *Anal. Chem.* **2016**, *88* (7), 3982–3989. https://doi.org/10.1021/acs.analchem.6b00225.

(20) Choi, C. H.; Kim, J.; Nam, J. O.; Kang, S. M.; Jeong, S. G.; Lee, C. S. Microfluidic Design of Complex Emulsions. *ChemPhysChem*. Wiley-VCH Verlag January 13, 2014, pp 21–29. https://doi.org/10.1002/cphc.201300821.

(21) Ma, Q.; Song, Y.; Sun, W.; Cao, J.; Yuan, H.; Wang, X.; Sun, Y.; Shum, H. C. Cell-Inspired All-Aqueous Microfluidics: From Intracellular Liquid–Liquid Phase Separation toward Advanced Biomaterials. *Adv. Sci.* **2020**, *7* (7), 1903359. https://doi.org/10.1002/advs.201903359.

(22) Shang, L.; Cheng, Y.; Zhao, Y. Emerging Droplet Microfluidics. *Chem. Rev.* **2017**, *117* (12), 7964–8040. https://doi.org/10.1021/acs.chemrev.6b00848.

(23) Linsenmeier, M.; Kopp, M. R. G.; Stavrakis, S.; de Mello, A.; Arosio, P. Analysis of Biomolecular Condensates and Protein Phase Separation with Microfluidic Technology. *Biochim. Biophys. Acta - Mol. Cell Res.* **2021**, *1868* (1), 118823. https://doi.org/10.1016/j.bbamcr.2020.118823.

(24) Albertsson, P.-Å. Partition of Cell Particles and Macromolecules in Polymer Two-Phase Systems. In *Advances in Protein Chemistry*; 1970; Vol. 24, pp 309–341. https://doi.org/10.1016/S0065-3233(08)60244-2.

(25) Albertsson, P.-Å. History of Aqueous Polymer Two-Phase Partition. In *Partitioning in Aqueous Two - Phase Systems*; Walter, H., Brooks, D. E., Fisher, D., Eds.; Academic Press:

Orlando, FL, 1985; pp 1–10.

(26) Iqbal, M.; Tao, Y.; Xie, S.; Zhu, Y.; Chen, D.; Wang, X.; Huang, L.; Peng, D.; Sattar, A.; Shabbir, M. A. B.; Hussain, H. I.; Ahmed, S.; Yuan, Z. Aqueous Two-Phase System (ATPS): An Overview and Advances in Its Applications. *Biol. Proced. Online* **2016**, *18* (1), 18. https://doi.org/10.1186/s12575-016-0048-8.

(27) Zaslavsky, B. Y.; Uversky, V. N.; Chait, A. Analytical Applications of Partitioning in Aqueous Two-Phase Systems: Exploring Protein Structural Changes and Protein–Partner Interactions in Vitro and in Vivo by Solvent Interaction Analysis Method. *Biochim. Biophys. Acta - Proteins Proteomics* **2016**, *1864* (5), 622–644. https://doi.org/10.1016/j.bbapap.2016.02.017.

(28) Teixeira, A. G.; Agarwal, R.; Ko, K. R.; Grant-Burt, J.; Leung, B. M.; Frampton, J. P. Emerging Biotechnology Applications of Aqueous Two-Phase Systems. *Adv. Healthc. Mater.* **2018**, *7* (6), 1701036. https://doi.org/10.1002/adhm.201701036.

(29) Silva, D. F. C.; Azevedo, A. M.; Fernandes, P.; Chu, V.; Conde, J. P.; Aires-Barros, M. R. Determination of Aqueous Two Phase System Binodal Curves Using a Microfluidic Device. *J. Chromatogr. A* **2014**, *1370*, 115–120. https://doi.org/10.1016/j.chroma.2014.10.035.

(30) Amine, C.; Boire, A.; Davy, J.; Marquis, M.; Renard, D. Droplets-Based Millifluidic for the Rapid Determination of Biopolymers Phase Diagrams. *Food Hydrocoll.* **2017**, *70*, 134–142. https://doi.org/10.1016/j.foodhyd.2017.03.035.

(31) Aumiller, W. M.; Keating, C. D. Experimental Models for Dynamic Compartmentalization of Biomolecules in Liquid Organelles: Reversible Formation and Partitioning in Aqueous

Biphasic Systems. *Adv. Colloid Interface Sci.* **2017**, *239*, 75–87. https://doi.org/10.1016/j.cis.2016.06.011.

(32) Grilo, A. L.; Raquel Aires-Barros, M.; Azevedo, A. M. Partitioning in Aqueous Two-Phase Systems: Fundamentals, Applications and Trends. *Sep. Purif. Rev.* **2016**, *45* (1), 68–80. https://doi.org/10.1080/15422119.2014.983128.

(33) Huddleston, J. The Molecular Basis of Partitioning in Aqueous Two-Phase Systems. *Trends Biotechnol.* **1991**, *9* (1), 381–388. https://doi.org/10.1016/0167-7799(91)90130-A.

(34) Johansson, H.-O.; Karlström, G.; Tjerneld, F.; Haynes, C. A. Driving Forces for Phase Separation and Partitioning in Aqueous Two-Phase Systems. *J. Chromatogr. B Biomed. Sci. Appl.* **1998**, *711* (1–2), 3–17. https://doi.org/10.1016/S0378-4347(97)00585-9.

(35) Silva, D. F. C.; Azevedo, A. M.; Fernandes, P.; Chu, V.; Conde, J. P.; Aires-Barros, M. R. Determination of Partition Coefficients of Biomolecules in a Microfluidic Aqueous Two Phase System Platform Using Fluorescence Microscopy. *J. Chromatogr. A* **2017**, *1487*, 242–247. https://doi.org/10.1016/j.chroma.2016.12.036.

(36) Vijayakumar, K.; Gulati, S.; DeMello, A. J.; Edel, J. B. Rapid Cell Extraction in Aqueous Two-Phase Microdroplet Systems. *Chem. Sci.* **2010**, *1* (4), 447. https://doi.org/10.1039/c0sc00229a.

(37) Asenjo, J. A.; Andrews, B. A. Aqueous Two-Phase Systems for Protein Separation: A Perspective. *J. Chromatogr. A* **2011**, *1218* (49), 8826–8835. https://doi.org/10.1016/j.chroma.2011.06.051.

(38) Bras, E. J. S.; Soares, R. R. G.; Azevedo, A. M.; Fernandes, P.; Arévalo-Rodríguez, M.;

Chu, V.; Conde, J. P.; Aires-Barros, M. R. A Multiplexed Microfluidic Toolbox for the Rapid Optimization of Affinity-Driven Partition in Aqueous Two Phase Systems. *J. Chromatogr. A* **2017**, *1515*, 252–259. https://doi.org/10.1016/j.chroma.2017.07.094.

(39) Vicente, F. A.; Plazl, I.; Ventura, S. P. M.; Žnidaršič-Plazl, P. Separation and Purification of Biomacromolecules Based on Microfluidics. *Green Chem.* **2020**, *22* (14), 4391–4410. https://doi.org/10.1039/C9GC04362D.

(40) Shin, H.; Han, C.; Labuz, J. M.; Kim, J.; Kim, J.; Cho, S.; Gho, Y. S.; Takayama, S.; Park, J. High-Yield Isolation of Extracellular Vesicles Using Aqueous Two-Phase System. *Sci. Rep.* **2015**, *5* (1), 13103. https://doi.org/10.1038/srep13103.

(41) Agarwal, R.; Liu, G.; Tam, N. W.; Gratzer, P. F.; Frampton, J. P. Precision Cell Delivery in Biphasic Polymer Systems Enhances Growth of Keratinocytes in Culture and Promotes Their Attachment on Acellular Dermal Matrices. *J. Tissue Eng. Regen. Med.* **2019**, *13* (6), term.2845. https://doi.org/10.1002/term.2845.

(42) Teixeira, A. G.; Kleinman, A.; Agarwal, R.; Tam, N. W.; Wang, J.; Frampton, J. P. Confinement of Suspension-Cultured Cells in Polyethylene Glycol/Polyethylene Oxide-Albumin Aqueous Two-Phase Systems. *Front. Chem.* **2019**, *7* (JUN). https://doi.org/10.3389/fchem.2019.00441.

(43) Yanagisawa, M.; Nigorikawa, S.; Sakaue, T.; Fujiwara, K.; Tokita, M. Multiple Patterns of Polymer Gels in Microspheres Due to the Interplay among Phase Separation, Wetting, and Gelation. *Proc. Natl. Acad. Sci.* **2014**, *111* (45), 15894–15899. https://doi.org/10.1073/pnas.1416592111.

(44) Zhao, H.; Ibrahimova, V.; Garanger, E.; Lecommandoux, S. Dynamic Spatial Formation and Distribution of Intrinsically Disordered Protein Droplets in Macromolecularly Crowded Protocells. *Angew. Chemie Int. Ed.* **2020**, *59* (27), 11028–11036. https://doi.org/10.1002/anie.202001868.

(45) Jia, T. Z.; Hentrich, C.; Szostak, J. W. Rapid RNA Exchange in Aqueous Two-Phase System and Coacervate Droplets. *Orig. Life Evol. Biosph.* **2014**, *44* (1), 1–12. https://doi.org/10.1007/s11084-014-9355-8.

(46) Aumiller, W. M.; Davis, B. W.; Keating, C. D. Phase Separation as a Possible Means of Nuclear Compartmentalization. In *International Review of Cell and Molecular Biology*; 2014; Vol. 307, pp 109–149. https://doi.org/10.1016/B978-0-12-800046-5.00005-9.

(47) Monterroso, B.; Zorrilla, S.; Sobrinos-Sanguino, M.; Keating, C. D.; Rivas, G. Microenvironments Created by Liquid-Liquid Phase Transition Control the Dynamic Distribution of Bacterial Division FtsZ Protein. *Sci. Rep.* **2016**, *6* (1), 35140. https://doi.org/10.1038/srep35140.

(48) Linsenmeier, M.; Kopp, M. R. G.; Grigolato, F.; Emmanoulidis, L.; Liu, D.; Zürcher, D.; Hondele, M.; Weis, K.; Capasso Palmiero, U.; Arosio, P. Dynamics of Synthetic Membraneless Organelles in Microfluidic Droplets. *Angew. Chemie - Int. Ed.* **2019**, *58* (41), 14489–14494. https://doi.org/10.1002/anie.201907278.

(49) Chen, Q.; Zhang, Y.; Chen, H.; Liu, J.; Liu, J. Enhancing the Sensitivity of DNA and Aptamer Probes in the Dextran/PEG Aqueous Two-Phase System. *Anal. Chem.* **2021**, *93* (24), 8577–8584. https://doi.org/10.1021/acs.analchem.1c01419.

(50) Jeyhani, M.; Gnyawali, V.; Abbasi, N.; Hwang, D. K.; Tsai, S. S. H. Microneedle-Assisted Microfluidic Flow Focusing for Versatile and High Throughput Water-in-Water Droplet Generation. *J. Colloid Interface Sci.* **2019**, *553*, 382–389. https://doi.org/10.1016/j.jcis.2019.05.100.

(51) Jeyhani, M.; Thevakumaran, R.; Abbasi, N.; Hwang, D. K.; Tsai, S. S. H. Microfluidic Generation of All-Aqueous Double and Triple Emulsions. *Small* **2020**, *16* (7), 1906565. https://doi.org/10.1002/smll.201906565.

(52) Moon, B.-U.; Jones, S. G.; Hwang, D. K.; Tsai, S. S. H. Microfluidic Generation of Aqueous Two-Phase System (ATPS) Droplets by Controlled Pulsating Inlet Pressures. *Lab Chip* **2015**, *15* (11), 2437–2444. https://doi.org/10.1039/C5LC00217F.

(53) Zhou, C.; Zhu, P.; Han, X.; Shi, R.; Tian, Y.; Wang, L. Microfluidic Generation of ATPS Droplets by Transient Double Emulsion Technique. *Lab Chip* **2021**, *21* (14), 2684–2690. https://doi.org/10.1039/D1LC00351H.

(54) Watanabe, T.; Motohiro, I.; Ono, T. Microfluidic Formation of Hydrogel Microcapsules with a Single Aqueous Core by Spontaneous Cross-Linking in Aqueous Two-Phase System Droplets. *Langmuir* **2019**, *35* (6), 2358–2367. https://doi.org/10.1021/acs.langmuir.8b04169.

(55) Ma, S.; Thiele, J.; Liu, X.; Bai, Y.; Abell, C.; Huck, W. T. S. Fabrication of Microgel Particles with Complex Shape via Selective Polymerization of Aqueous Two-Phase Systems. *Small* **2012**, *8* (15), 2356–2360. https://doi.org/10.1002/smll.201102715.

(56) Cui, C.; Zeng, C.; Wang, C.; Zhang, L. Complex Emulsions by Extracting Water from

Homogeneous Solutions Comprised of Aqueous Three-Phase Systems. *Langmuir* **2017**, *33* (44), 12670–12680. https://doi.org/10.1021/acs.langmuir.7b02888.

(57) Douliez, J.-P.; Martin, N.; Beneyton, T.; Eloi, J.-C.; Chapel, J.-P.; Navailles, L.; Baret, J.-C.; Mann, S.; Béven, L. Preparation of Swellable Hydrogel-Containing Colloidosomes from Aqueous Two-Phase Pickering Emulsion Droplets. *Angew. Chemie* **2018**, *130* (26), 7906–7910. https://doi.org/10.1002/ange.201802929.

(58) DeJournette, C. J.; Kim, J.; Medlen, H.; Li, X.; Vincent, L. J.; Easley, C. J. Creating Biocompatible Oil–Water Interfaces without Synthesis: Direct Interactions between Primary Amines and Carboxylated Perfluorocarbon Surfactants. *Anal. Chem.* **2013**, *85* (21), 10556–10564. https://doi.org/10.1021/ac4026048.

(59) Gruner, P.; Riechers, B.; Chacòn Orellana, L. A.; Brosseau, Q.; Maes, F.; Beneyton, T.; Pekin, D.; Baret, J. C. Stabilisers for Water-in-Fluorinated-Oil Dispersions: Key Properties for Microfluidic Applications. *Current Opinion in Colloid and Interface Science*. Elsevier June 1, 2015, pp 183–191. https://doi.org/10.1016/j.cocis.2015.07.005.

(60) Holtze, C.; Rowat, A. C.; Agresti, J. J.; Hutchison, J. B.; Angilè, F. E.; Schmitz, C. H. J.; Köster, S.; Duan, H.; Humphry, K. J.; Scanga, R. A.; Johnson, J. S.; Pisignano, D.; Weitz, D. A. Biocompatible Surfactants for Water-in-Fluorocarbon Emulsions. *Lab Chip* **2008**, *8* (10), 1632. https://doi.org/10.1039/b806706f.

(61) Gruner, P.; Riechers, B.; Semin, B.; Lim, J.; Johnston, A.; Short, K.; Baret, J. C. Controlling Molecular Transport in Minimal Emulsions. *Nat. Commun.* **2016**, *7* (1), 10392. https://doi.org/10.1038/ncomms10392.

(62) Abate, A. R.; Thiele, J.; Weitz, D. A. One-Step Formation of Multiple Emulsions in Microfluidics. *Lab Chip* **2011**, *11* (2), 253–258. https://doi.org/10.1039/c0lc00236d.

(63) Invitrogen. Concanavalin A Conjugates https://assets.thermofisher.com/TFS-Assets/LSG/manuals/mp00825.pdf (accessed Jul 2, 2021).

(64) Liu, Y. F.; García, A. A. Three Phase Countercurrent Extraction. *Chem. Eng. Commun.* **2000**, *182* (1), 239–259. https://doi.org/10.1080/00986440008912836.

(65) Albertsson, P. A. Application of the Phase Partition Method to a Hydrophobic Membrane Protein, Phospholipase Al from Escherichia Coli. *Biochemistry* **1973**, *12* (13), 2525–2530. https://doi.org/10.1021/bi00737a024.

(66) Baskir, J. N.; Hatton, T. A.; Suter, U. W. Protein Partitioning in Two-Phase Aqueous Polymer Systems. *Biotechnol. Bioeng.* **1989**, *34* (4), 541–558. https://doi.org/10.1002/bit.260340414.

(67) Brooks, D. E.; Sharp, K. A.; Fisher, D. Theoretical Aspects of Partitioning. In *Partitioning in Aqueous Two - Phase Systems*; Walter, H., Brooks, D. E., Fisher, D., Eds.; Academic Press: Orlando, FL, 1985; pp 11–84.

For Table of Contents Only: